JGR Atmospheres

RESEARCH ARTICLE
10.1029/2024JD042584

Ice-Nucleating Particles Are Emitted by Raindrop Impact

C. Mignani[1,2], T. C. J. Hill[1], M. Nieto-Caballero[1], K. R. Barry[1], N. C. Bryan[1,3], P. J. Marinescu[1], B. Dolan[1], A. P. Sullivan[1], M. Hernandez[4], A. Bosco-Lauth[5], S. C. van den Heever[1], E. A. Stone[6], L. D. Grant[1], R. J. Perkins[1], P. J. DeMott[1], and S. M. Kreidenweis[1]

[1]Department of Atmospheric Science, Colorado State University, Fort Collins, CO, USA, [2]Water and Soil Resource Research, Institute of Geography, University of Augsburg, Augsburg, Germany, [3]Now at Brigham and Women's Hospital, Boston, MA, USA, [4]Department of Civil, Environmental and Architectural Engineering, University of Colorado, Boulder, CO, USA, [5]Department of Biomedical Sciences, Colorado State University, Fort Collins, CO, USA, [6]Department of Chemistry, University of Iowa, Iowa City, IA, USA

Abstract Ice-nucleating particles (INPs) play a key role in ice formation and cloud microphysics and thus significantly impact the water cycle and the climate. However, our understanding of atmospheric INPs, particularly their sources, emissions, and spatiotemporal variability, is incomplete. While the enhancement of atmospheric INP concentrations with rainfall has been previously shown, a mechanistic understanding of the process is lacking. Here, we link detailed precipitation observations with near-surface atmospheric INP concentrations at a semiarid grassland site in Colorado. Considering the during-precipitation air samples, INP concentrations positively correlate with cumulative rainfall kinetic energy and amount, suggesting that INP aerosolization is induced by raindrop and hailstone impact. By additionally analyzing the INP content of precipitation water, terrestrial source samples, and heat-treated samples, we demonstrate that local plants are the most plausible source of rain-induced INPs during a precipitation event. Should INPs aerosolized by precipitation rise to cloud height, they could influence cloud ice fraction and initiate precipitation resulting in an aerosol-cloud-precipitation feedback.

Plain Language Summary Ice-nucleating particles (INPs) are natural particles released from the land surface that play a key role in ice formation in clouds, the initiation step for the formation of precipitation in many clouds and a factor in how clouds warm or cool the atmosphere through scattering and absorbing solar and terrestrial radiation. Previously, unusual enhancement of atmospheric INP concentrations has been associated with rainfall, but a mechanistic understanding of the process has not been confirmed. Using detailed observations of precipitation and near-surface atmospheric INP concentrations, INP concentrations during rainfall are found to correlate with cumulative rainfall kinetic energy and amount, suggesting that INP aerosolization is induced by raindrop and hailstone impact. By additionally analyzing the INP contents of precipitation water and terrestrial source samples, and their thermal stability, it is demonstrated that local plant surfaces are the most important source of rain-induced INPs during a precipitation event. While this study occurred at a semiarid grassland site in Colorado, USA, it can be expected to be active in any ecosystem. INPs aerosolized by precipitation that reach cloud heights could affect how precipitation develops. Results provide a potential mechanistic link for implementation in numerical models to study land-atmosphere-precipitation interactions.

Key Points:

- The impact of rain and hail on land aerosolizes ice-nucleating particles (INPs)
- Atmospheric INP concentrations during rainfall correlate with cumulative rainfall kinetic energy and cumulative rainfall amount
- Detailed analyses of one prominent case suggest local vegetation as the most plausible source of rain-induced atmospheric INPs

Supporting Information:

Supporting Information may be found in the online version of this article.

Correspondence to:

C. Mignani,
claudia.mignani@colostate.edu

Citation:

Mignani, C., Hill, T. C. J., Nieto-Caballero, M., Barry, K. R., Bryan, N. C., Marinescu, P. J., et al. (2025). Ice-nucleating particles are emitted by raindrop impact. *Journal of Geophysical Research: Atmospheres*, *130*, e2024JD042584. https://doi.org/10.1029/2024JD042584

Received 30 SEP 2024
Accepted 21 MAY 2025

Author Contributions:

Conceptualization: C. Mignani, T. C. J. Hill, P. J. DeMott, S. M. Kreidenweis
Data curation: C. Mignani, T. C. J. Hill, K. R. Barry, P. J. Marinescu, R. J. Perkins, P. J. DeMott, S. M. Kreidenweis
Formal analysis: C. Mignani, T. C. J. Hill
Funding acquisition: C. Mignani, A. Bosco-Lauth, S. C. van den Heever, E. A. Stone, L. D. Grant, R. J. Perkins, P. J. DeMott, S. M. Kreidenweis
Investigation: C. Mignani, T. C. J. Hill, M. Nieto-Caballero, N. C. Bryan, L. D. Grant, R. J. Perkins, P. J. DeMott, S. M. Kreidenweis
Methodology: C. Mignani, T. C. J. Hill, M. Nieto-Caballero, K. R. Barry,

1. Introduction

After finding a bacterium in an ice crystal residue, Soulage suggested as early as 1957 that biological ice-nucleating particles (INPs) are involved in the freezing of cloud droplets (Soulage, 1957). Three decades later, the pioneering concept now known as the "bioprecipitation cycle" was introduced (Morris et al., 2014; Sands et al., 1982), in which rainfall serves as a mechanism to aerosolize biological INPs that can rise to cloud height where they can initiate rain. This hypothesis was supported by the identification of the potential plant pathogen, *Pseudomonas syringae*, strains of which have an ice nucleation-active protein located in the outer cell membrane (Wolber et al., 1986). These strains are more abundant on plants after intense rainfall (Hirano et al., 1996) and have the ability to freeze water droplets at unusually warm temperatures, with the warmest value reported being −1.2°C (Lindow et al., 1989). Meanwhile, a variety of biological INPs with different freezing mechanisms and activation temperatures originating from surfaces such as soils, plants, and waters have been identified (Huang

N. C. Bryan, P. J. DeMott, S. M. Kreidenweis
Project administration: C. Mignani, A. Bosco-Lauth, S. C. van den Heever, E. A. Stone, L. D. Grant, R. J. Perkins, P. J. DeMott, S. M. Kreidenweis
Resources: C. Mignani, T. C. J. Hill, K. R. Barry, P. J. Marinescu, B. Dolan, A. P. Sullivan, M. Hernandez, S. C. van den Heever, L. D. Grant, R. J. Perkins, P. J. DeMott, S. M. Kreidenweis
Software: C. Mignani, T. C. J. Hill, K. R. Barry, P. J. Marinescu, R. J. Perkins
Supervision: S. C. van den Heever, E. A. Stone, L. D. Grant, R. J. Perkins, P. J. DeMott, S. M. Kreidenweis
Validation: C. Mignani, T. C. J. Hill, M. Nieto-Caballero, B. Dolan, E. A. Stone, R. J. Perkins, P. J. DeMott, S. M. Kreidenweis
Visualization: C. Mignani
Writing – original draft: C. Mignani
Writing – review & editing: C. Mignani, T. C. J. Hill, M. Nieto-Caballero, K. R. Barry, N. C. Bryan, P. J. Marinescu, B. Dolan, A. P. Sullivan, M. Hernandez, A. Bosco-Lauth, S. C. van den Heever, E. A. Stone, L. D. Grant, R. J. Perkins, P. J. DeMott, S. M. Kreidenweis

et al., 2021). Biological INPs tend to have a greater freezing efficiency at temperatures warmer than −15°C than mineral INPs (Murray et al., 2012). While they maybe present in small number concentrations in clouds, their activation leads to the formation of ice crystals, which can multiply (Korolev & Leisner, 2020) and are a prerequisite for a large fraction of precipitation globally (Mülmenstädt et al., 2015). This underlines the need for increased observation of biological INPs (Burrows et al., 2022; DeMott & Prenni, 2010).

Based on recent evidence, INPs active at temperatures ≥−20°C (warm-temperature INPs) are predominantly biological aerosol particles (Cornwell et al., 2023; Pereira Freitas et al., 2023). Therefore, their abundance cannot be expected to be strongly related to the number concentrations of the general aerosol population (DeMott et al., 2010; Mignani et al., 2021; Testa et al., 2021; Tobo et al., 2013). Atmospheric warm-temperature INP concentrations vary substantially and are enhanced during rainfall. Some of the earliest evidence of increased INP concentrations associated with precipitation events was observed in Australia, Japan, the United States, and Canada (Bigg, 1958; Isaac & Douglas, 1973; Isono & Tanaka, 1966; Ryan & Scott, 1969). Investigations conducted during summertime in a Colorado pine forest further advanced the understanding of the INP enhancement associated with rainfall by showing concurrent increases of bioaerosol particles (Huffman et al., 2013; Prenni et al., 2013; Tobo et al., 2013) by using high-temporal-resolution online INP measurements, fluorescence detection, and microscopy techniques. In addition, the enhancement of INPs with precipitation has been reported for different seasons and various regions using drop freezing methods (Conen et al., 2017; Gong et al., 2022; Hara et al., 2016; Mignani et al., 2021; Testa et al., 2021). Some of these studies distinguished between periods with rain and no rain at the observation site (Huffman et al., 2013; Testa et al., 2021; Tobo et al., 2013) have included precipitation history along sampled air masses (Gong et al., 2022; Mignani et al., 2021), or considered local rainfall intensity (Conen et al., 2017; Hara et al., 2016; Isaac & Douglas, 1973; Isono & Tanaka, 1966; Prenni et al., 2013; Testa et al., 2021). Schneider et al. (2021) observed rain-induced increases in INP concentrations only during two of the strongest precipitation events (i.e., roughly 0.6 mm) in June and September in a boreal forest in Finland. The "rain-induced enhancement of INP concentrations may have been missed" because of longer sampling times (i.e., 24–144 hr) according to the authors.

Aerosol particles can be emitted through the impact of raindrops, in addition to wind dispersal and active emission processes (Fröhlich-Nowoisky et al., 2016). Aerosolization via raindrop impact has been observed from both plant leaves and soils under laboratory settings using high-speed imaging techniques (Gilet & Bourouiba, 2014; Joung et al., 2017; Kim et al., 2019; Nath et al., 2019). This mechanism depends on, among other factors, the microphysics of precipitation (i.e., the physical properties of raindrops). However, a causal mathematical relationship between precipitation parameters and the emission of INPs has not been established. Today, precipitation measurements characterizing ground-based precipitation microphysics are available, using laser-based instruments like a particle size and velocity (Parsivel) disdrometer (Löffler-Mang & Joss, 2000). Such techniques have already been applied in studies where understanding, representing, or predicting rainfall parameters is of interest, such as in atmospheric and soil erosion sciences (Dolan et al., 2018; Wilken et al., 2018). Quantifying the relationship between rainfall and INPs could facilitate the inclusion of rainfall as a driver of INPs in numerical models, which typically use only aerosol particle-dependent INP parameterizations to date (Burrows et al., 2022). As the probability of heavy precipitation increases due to climate change (Fischer & Knutti, 2016), it is particularly interesting to better understand and represent the interplay between aerosol particles, clouds, and precipitation.

Here, we have collected samples at a northern Colorado semiarid grassland site during two spring periods over several weeks and 15 precipitation events. We have collected high-volume filter samples ($n = 66$) at approximately 1.5 m above ground with high temporal resolution, focusing on sampling before, during, and after precipitation. Our primary goal was to investigate INP concentrations across precipitation events. We analyzed the relationship between INP concentrations and detailed precipitation characteristics leveraging disdrometer observations. In addition, we assessed potential sources of rain-induced atmospheric INPs by analyzing precipitation water ($n = 15$) and terrestrial source ($n = 3$) samples. We provide new, fundamental insights into factors affecting INP variability near the Earth's surface for continental, temperate, semiarid grassland environments, although we expect that these findings can be translated to better understand atmospheric INPs over other ecosystems.

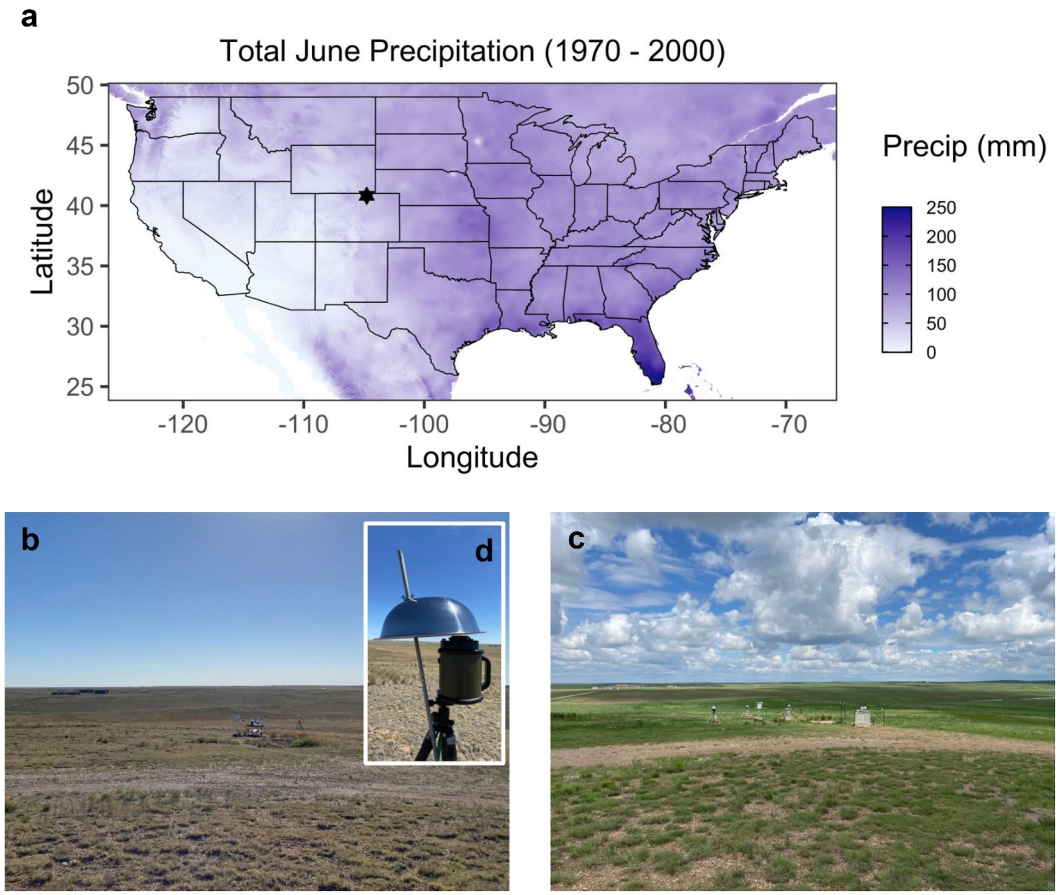

Figure 1. Sampling site overview. (a) Geographical location of the sampling site (black star) and average total precipitation (mm) for the month of June (1970–2000) for the USA (Fick & Hijmans, 2017). Sampling site in June 2022 (b) and June 2023 (c). SASS® 3100 sampler with a precipitation shield on a tripod (d). Note that the instruments are in the same location in 2022 and 2023.

2. Materials and Methods

We present observations collected within the Central Plains Experimental Range (CPER) near Nunn, Colorado, USA, during late May–late June in both 2022 and 2023. The CPER, administered by the U.S. Department of Agriculture, is located in the intermittently grazed shortgrass prairie of the North American Great Plains and is in the rain shadow of the Rocky Mountains, with an average historical (1970–2000) June total precipitation of about 54 mm, as depicted in Figure 1a. Sampling took place during the BioAerosols and Convective Storms (BACS) and the Biology Integration Institute: Regional OneHealth Aerobiome Discovery Network (BROADN) field campaigns and was coordinated with the National Ecological Observing Network (NEON), which operates a site within CPER. The data collection occurred during two consecutive spring periods that produced very different amounts of precipitation. In June 2022, total precipitation was only 12 mm, while in June 2023, it reached 125 mm, as indicated by monthly U.S. Climate Reference Network (USCRN) data from a monitoring station near Nunn, CO, situated 1.9 km east of the sampling site (from now on referred to as nearby USCRN station; Diamond et al., 2013). This substantial interannual variation in precipitation had profound effects on vegetation cover at CPER and in its surrounding area (see comparison of 28 June 2022 and 2023 of the MODIS Corrected Reflectance product here: https://go.nasa.gov/456uTXZ, last access: 26 September 2024). In 2022, the landscape consisted mainly of bare soil, dry grasses, and a minimal new growth on perennial small shrubs and cacti, whereas in 2023, it was green, mainly due to lush growth of grasses, and larger and more verdant shrub canopies (Figures 1b and 1c). Notably, in a statistical analysis of daily rainfall time series (Morris et al., 2017; Soubeyrand et al., 2014) characterizing rainfall feedbacks of nearly 3,000 sites in the USA, the CPER area was identified as having a positive rainfall feedback (see http://w3.avignon.inra.fr/rainfallfeedback/, last access: 26 September

2024); a positive rainfall feedback was characterized as a precipitation event followed by a higher frequency of subsequent rain events over 20 days than expected on average and is indicative of a self-sustaining nature of wet periods at a site, or vice versa.

2.1. Sampling Descriptions

Sampling occurred at ground level in a native landscape (40.810°N, 104.778°W; 1,660 m above sea level, Figure 1) in close proximity to the Semi-arid Grassland Research Center (SGRC), jointly operated by Colorado State University and the U. S. Department of Agriculture. We sampled aerosol particles, precipitation, and other potential terrestrial INP sources (i.e., soil, surface water and leaf water).

Aerosol particles were collected on filters with samplers that were mounted on tripods at 1–2 m above ground, and included stainless steel precipitation shields. We used a SASS® 3100 sampler (Research International) operating at 300 L min^{-1} and associated removable 44-mm bioaerosol electret filters (here referred to as SASS filters; product number: 7100-134-232-01; Figure 1d). In 2023, the SASS filters were sterilized with ethylene oxide before use, a step that did not change the background INP levels of field blanks (Figure S1 in Supporting Information S1). The collection efficiencies of these SASS filters are >50%, >70%, and >90% for particles of about 0.4 μm, 0.8 μm, and 2.5 μm in size, respectively (internal report by Research International). The SASS sampler was deployed with the filter inlet facing upward and the air outlet oriented so that the air blew in a similar direction as the prevailing wind. The SASS filters were collected over an average period of 2.6 hr and a standard deviation of 1.6 hr, with a minimum of 26 min and a maximum of 9 hr (Table S1 in Supporting Information S1). They were removed in the field using sterile, disposable forceps (TWD Scientific) and stored in sterile Petri dishes (Pall Corporation), sealed with Parafilm®, and wrapped in aluminum foil. To ensure sterile fieldwork, we decontaminated surfaces, such as the filter holder and the gloves, with DNA AWAY® Surface Decontaminant (Molecular BioProducts) before use, positioned ourselves downwind of the samples during filter changes, and started the sampler running with a 15-s delay. In addition, polycarbonate (PC) filter samples were collected at the same location in 2022 using single-use open-face sterile plastic filter units (Nalgene, Waltham) with precleaned 0.2-μm pore size, 47-mm Nuclepore PC filters (Whatman, GE Healthcare) as done previously (Beall et al., 2021; Testa et al., 2021). For the PC filter collection, we used a vacuum pump (Model 2688CE44, Thomas) with a mean flow rate of approximately 14 L min^{-1} at standard temperature and pressure (STP, i.e., 0°C and 1,013.25 mbar). Mean flow was calculated based on measurements at the beginning and the end of sampling using a flow meter (5,200 series, TSI). All particle sizes are expected to be collected with 100% efficiency on the PC filters except those between 0.02 and 0.2 μm in diameter, a size window for which the collection efficiency drops to a minimum value of about 70% for 0.1 μm-particles (Spurny & Lodge, 1972). The PC filters were removed in a portable laminar flow hood using cleaned plastic forceps (Fine Science Tools) and stored in sterile Petri dishes (Pall Corporation). The collection of PC filter samples was done concurrently with sampling of representative SASS filter samples. The use of SASS filters for determination of INP concentrations was validated against the well-established method using PC filters, with findings shown in Figure S2 in Supporting Information S1. We found that the results of the two filter types were in agreement across the analyzed temperature spectrum. The PC filters generally showed slightly higher INP values than colocated SASS filters for coinciding time windows, but the differences were within a factor of five or less. This could be due to the PC filters collecting all particle sizes more efficiently than SASS filters. Overall though, the results of the SASS filters match those of the PC filters quite well across a wide dynamic concentration and temperature range. We therefore expect our results to be independent of the filter type. Notably, Figure S2 in Supporting Information S1 is the only one that includes results from PC filters; therefore, air or filter samples in this work refer to SASS filter samples.

Rain, including occasional hail, was collected during each precipitation event (i.e., precipitation event defined in Section 2.4 (*Sampling strategy […]*), see Table S1 in Supporting Information S1). Prior to the occurrence of precipitation, large disposable plastic bags (Ziploc® Big Bag XL, individually repacked) were freshly opened and carefully inserted, while wearing gloves and sleeves, into the sample container of the atmospheric deposition sampler (ADS 00-120, N-CON Systems) with a collection container of 29 cm in diameter. The sampler automatically opened and closed when precipitation was detected by a sensor in the device. Shortly after precipitation fell, the precipitation water (rain or rain and melted hail stones) was transferred for storage, weighed, and frozen. On average, 148 mL of water per precipitation sample were collected, with a minimum of 11 mL and a maximum of 588 mL. For INP measurements, we filled a sterile 50-mL polypropylene Corning® centrifuge tube (hereafter a 50-mL tube) with precipitation water, sealed it with Parafilm, and wrapped it in aluminum foil.

In 2022, one topsoil sample was collected from a representative soil cover (i.e., a mixture of bare soil, grass, shrubs, and cacti). Soil from three different, proximate spots was scraped from the surface (0–1 cm) and placed into a 50-mL tube. In 2023, surface water was collected from various ponds formed after precipitation using 20-mL syringes and transferred to 50-mL tubes. Additionally, we collected one plant leaf water sample during light rain from *Artemisia frigida* (or prairie sagebrush). This drought-tolerant shrub, common at the site, has green gray linear leaves about 1.5 cm in length covered with silky white hairs. Raindrops adhering to the hydrophobic plant were sampled individually with a 20-mL syringe until a total of approximately 5 mL of water was collected. Then, the water was poured into 50-mL tubes. After sampling, all samples were immediately stored at −20°C until processing.

2.2. Immersion Freezing Ice-Nucleating Particle (INP) Measurements

The INP concentrations for our samples were determined using the Colorado State University ice spectrometer (IS) (Demott et al., 2018). The IS analyzes liquid suspensions for immersion freezing across subzero temperatures, typically down to approximately −29°C. INP estimates were derived using a well-established protocol (Barry, Hill, Levin, et al., 2021; Testa et al., 2021), with minor adaptations tailored for SASS filter analysis, which was applied for INP measurements for the first time in this study. In the laboratory, we strictly followed the clean working methods described by Barry, Hill, Jentzsch, et al. (2021), which included processing samples in a laminar flow hood. To resuspend aerosol particles from the SASS filters, we first quartered the filters using scissors (Fine Science Tools), which were rinsed with deionized water (DI), decontaminated with DNA AWAY® Surface Decontaminant, and left to dry within the laminar flow hood before use. We then placed one–three filter quarters into cleaned 50-mL tubes and added 6–8 mL of DI, which was filtered through 0.1-μm syringe filters (Puradisc, Whatman, GE Healthcare). The tubes were then subjected to seven 10-s swirling cycles using a vortex mixer (Thermo Scientific) set at 3,000 revolutions per minute (RPM). The same was done for PC filters, except that the whole filters were used for suspensions, and the tubes were tumbled for 20 min (instead of vortexing) using a previously described method (Barry, Hill, Levin, et al., 2021; Testa et al., 2021). Precipitation water samples, as well as samples of surface water and leaf water, were melted at room temperature while tumbled with the rotator at roughly 5 RPM. Typically, four serial dilutions were prepared from the undiluted sample in 11-fold steps, and the suspensions of usually 32 aliquots of 50 μL were dispensed into polymerase chain reaction (PCR) plates (OPTIMUM® μLTRA brand, Life Science Products). Note that for each sample, the DI used for the suspension was also analyzed and used as background. The soil suspension was prepared by combining 5 g of thoroughly mixed thawed soil sample with DI to reach a final volume of 20 mL. The mixture was then gently tumbled for 20 min. Subsequently, 3 mL of this suspension were diluted to a total volume of 30 mL. This resulting suspension was used for distribution into PCR plates for IS measurements as well as four serial 20-fold dilutions.

The filled PCR plates were placed in aluminum blocks in the IS at room temperature and then were continuously cooled at 0.33°C min^{-1}. Freezing of the wells was determined optically in 0.1–0.5-degree steps from periodically taken images, which were automatically analyzed using custom-written LabVIEW code (Perkins et al., 2020) and manually checked for accuracy. Some unrecognized freezing events, which occurred particularly at high temperatures (typically above −10°C) had to be detected and added manually. Cumulative INP concentrations per unit liquid of the sample were calculated using the Vali equation (Equation 13 in Vali, 1971), and then converted to our chosen unit volume. To standardize the INP concentration, both aerosol and precipitation water samples were converted to units per standard liter of air. For SASS filters, this involved determining the collected volume at STP using the temperature and pressure measured at a nearby weather station averaged over each filter collection period (as specified in Section 2.3 (*Precipitation measurements […]*)). For precipitation water samples, 0.4 g of cloud water per 1000 L of air were assumed as in Petters and Wright (2015). The uncertainty in this estimate was stated as a factor of two on the basis of the range of cloud water contents associated with precipitating clouds (Petters & Wright, 2015), although the appropriate value of cloud water content related to precipitation from convective clouds at this site is not known.

For selected samples, we conducted several analyses to determine the characteristics of INPs. Initially, the suspended sample was diluted by a factor of two. Subsequently, 2 mL of the diluted sample were subjected to two treatments to investigate INP characteristics: heat treatments or hydrogen peroxide (H_2O_2) digestion. The suspension underwent heat treatment for 20 min, following the method outlined in Hill et al. (2016), to test for heat sensitivity. Here, this included exposure to two different temperatures: 50°C and 95°C. Furthermore, we conducted an H_2O_2 digestion using a 10% H_2O_2 suspension, and including heating to 95°C and exposure to UV-B

light, as described in detail in Suski et al. (2018). The INPs that withstand the H_2O_2 digestion provide an estimate of the inorganic INPs (i.e., of mineral origin), while those eliminated provide an estimate of organic INPs. Note that organic INPs are often subdivided into heat-labile biological and other organic INPs based on wet heating above 90°C (Hill et al., 2016; Knopf et al., 2021; Suski et al., 2018), because different organic INPs exhibit varying levels of temperature tolerance before losing their ice-nucleating ability. Because we determined heat sensitivity at two temperatures, we refer to specific temperature-dependent heat-labile INPs (i.e., 50°C heat- and 95°C heat-labile INPs). As summarized in a table in Conen et al. (2022), certain INPs derived from bacteria or fungi are considered heat-labile at low heat (i.e., ≤60°C). Conversely, INPs from pollen or lignin display remarkable heat resistance, remaining functional even at temperatures as high as 95°C, and organic INPs obtained from soils and decaying leaves generally withstand low heat but experience a significant reduction in ice-nucleating activity ≥−15°C when exposed to temperatures close to boiling.

Background INP concentrations of SASS filters and precipitation bags were determined by collecting background samples in the field, using the same handling and analyzing procedure as for the samples. The only difference is that, for background air sampling, we placed a filter on the sampler holder for a few seconds without pulling air through it, and for background precipitation sampling, we inserted a plastic bag into the bucket of the deposition sampler and poured ultrapure water (nuclease-free water, Sigma-Aldrich) into it. For INPs active at −27°C, field blank SASS filters contained less than 10,000 INPs per filter, whereas a field blank plastic bag contained less than 100 INPs per bag (Figure S1 in Supporting Information S1), the latter being comparable to values reported for other plastic bags (Barry, Hill, Jentzsch, et al., 2021). Because background values accounted for only a smaller percentage of the INPs per sampling unit (i.e., filter or bag) than those of the respective samples, they were considered negligible.

For this study, a total of 66 SASS filter samples, 6 PC filter samples, 15 precipitation water samples, 3 terrestrial source samples (soil, surface water, and leaf water), 5 background SASS filters, and 1 precipitation blank were analyzed for INP measurements via immersion freezing using the IS.

2.3. Precipitation Measurements, Other Meteorological Parameters, and Weather Forecasts

The cumulative precipitation amount (or total precipitation, sumP) was calculated by dividing the total precipitation water volume collected with the deposition sampler by its horizontal area. We used a bag inside the sampling container (to collect the precipitation water for further analysis, see Section 2.1 (*Sampling descriptions*)) and thus a diameter of 28 cm, accounting for the container's diameter and a 1-cm diameter loss due to imperfect bag fitting. During the 2023 campaign, we expanded these precipitation measurements by deploying an OTT Parsivel^2 disdrometer (OTT HydroMet). This laser-based instrument detects falling hydrometeors, categorizing them into 32 size and velocity classes. A detailed description of this instrument can be found in the literature (e.g., Löffler-Mang & Joss, 2000; Tokay et al., 2014) or in the user manual (OTT HydroMet, 2017). The disdrometer was positioned a few meters from the atmospheric samplers, at a laser height of approximately 1.5 m above the ground. It operated continuously, collecting data at 30-s intervals, with occasional interruptions due to a defective RS-485/USB interface converter. The manufacturer's postprocessing software provided 30-s resolved precipitation microphysical parameters derived from the raw data (i.e., velocity and size bins of hydrometeors), such as precipitation amount (P), precipitation intensity (PI), kinetic energy (KE), number of hydrometeors (N), and the type of precipitation via weather code. We worked with the software output and determined the sum, mean, or maximum of selected precipitation parameters for relevant time windows that coincided with the air sampling. Note that KE is the KE of all the hydrometeors per measuring area and per time interval, and the cumulative KE (sumKE) is the sum of the 30-s resolved KE values over the air sampling period.

In addition, we computed the sumP (sum of total precipitation over the air sampling periods) using five-minute resolved observations of precipitation obtained from a weighing bucket gauge, obtained from the nearby USCRN station (Diamond et al., 2013). The sumP determined using the deposition sampler closely matched those calculated using the disdrometer (Figure S3a in Supporting Information S1), affirming the reliability of both measurement approaches. Nevertheless, it is important to note that the disdrometer has a higher sensitivity when measuring lower amounts of precipitation. In six sampling time windows where precipitation was captured by the disdrometer, we were unable to determine precipitation amount with the deposition sampler. The lowest sumP was 0.001 mm using the disdrometer whereas it was 0.18 mm from the deposition sampler. When comparing sumP measured at the sampling site with data from the nearby USCRN station (for the same time windows), there

were noticeable differences (Figure S3b in Supporting Information S1). This inconsistency can most likely be attributed to the often convective, and thus highly spatially and temporally variable, nature of the raining storms observed during our study (see Krajewski et al., 2003). Hence, we only relied on precipitation measurements conducted at the sampling site.

In addition, one-minute mean values of air temperature and pressure were retrieved from the NEON measurement tower (Metzget et al., 2019), located 2.7 km east of the sampling site. Mean values were calculated over the filter sampling time windows and were used to calculate cumulative INP concentrations for SASS filters expressed in standard liters of air.

Some members of the BACS team provided site-specific weather forecasts each morning. Forecasts were based on radiosonde data and numerical weather predictions from multiple models. These forecasts helped to decide whether sampling would be carried out on a particular day. The start and stop times for air and precipitation sampling (Table S1 in Supporting Information S1) were determined throughout the day, guided by frequent on-site weather observations and real-time radar images obtained through the use of RadarScope® (DNT), a weather radar visualization application.

2.4. Sampling Strategy and Definitions of Precipitation Events and Samples

Our sampling strategy was to collect samples before, during, and after storms, defined here as precipitation events (Table S1 in Supporting Information S1). Due to this sampling strategy, samples were primarily taken on days with an unstable atmosphere and convection. When precipitation fell, it often originated from convective storms that passed the site in the afternoon or evening. A precipitation event ideally includes three air samples: a pre-precipitation sample, a during-precipitation sample, and a postprecipitation sample, along with one precipitation water sample. We defined an air sample as one during precipitation when precipitation occurred at the site during sampling. As described above, precipitation was detected with the disdrometer (sumP $\geq$ 0.001 mm), or the less-sensitive bag method if disdrometer data were not available. This classification resulted in a few cases where more than one during-precipitation air sample was collected per event (Table S1 in Supporting Information S1). Therefore, the number of samples per event varied. Also, if a storm occurred in the evening hours, a post-precipitation air sample was often not taken in order to avoid the need for night sampling. If there was a risk of lightning strikes, the filter change was delayed until access to the sampler was considered safe, sometimes leading to the integration of a preprecipitation into a during-precipitation air sample. Ultimately, we considered a precipitation event to be a sequence of successive air samples that included at least one during-precipitation air sample and a coinciding precipitation water sample. Note that no more than one precipitation event was considered per day. A total of 15 precipitation events were sampled, four events in 2022 for which a total of 5.8 mm precipitation was measured, and 11 events in 2023 with a total of 29.3 mm precipitation (Table S1 in Supporting Information S1). The minimum and maximum sumP measured during-precipitation air samples was 0.001 and 9.56 mm, respectively (Table S1 in Supporting Information S1).

3. Results

3.1. INP Concentrations in Air and Precipitation Water

Most INP concentrations in air and precipitation water analyzed in this study were within the range of previously reported air and precipitation samples (Kanji et al., 2017; Petters & Wright, 2015) (Figure 2). At the inflection point of cumulative INP spectra around −20°C and colder, the distribution of air samples followed a log-linear distribution (Figure 2a). Warmer than approximately −20°C, the vast majority of air samples exhibited semilog-linear distributions, including a minor "hump," characterized by a steeper increase at temperatures warmer than −10°C and a flatter rate of increase from −10°C to −20°C. However, a subset of samples deviated from this pattern, displaying a moderate to pronounced hump in INP concentrations between −5°C and −20°C. A few of these showed an extremely steep increase in INP concentrations between −5°C and −9°C, followed by near-stagnant concentrations from −10°C to −20°C. The hump is a feature that has been previously shown to be mainly caused by 95°-C-heat-labile INPs (Hill et al., 2016; Knopf et al., 2021; Suski et al., 2018). Notably, those observed here contained remarkably high INP concentrations at freezing temperatures between −5°C and −12°C. At −10°C, the maximum INP concentration was 2.4 per STP L^{-1} air. In literature, greater respective concentrations were only reported in perturbed harvesting scenarios (Garcia et al., 2012). During-precipitation air samples exhibited INP concentrations similar to pre- and postprecipitation air at temperatures below −20°C, but

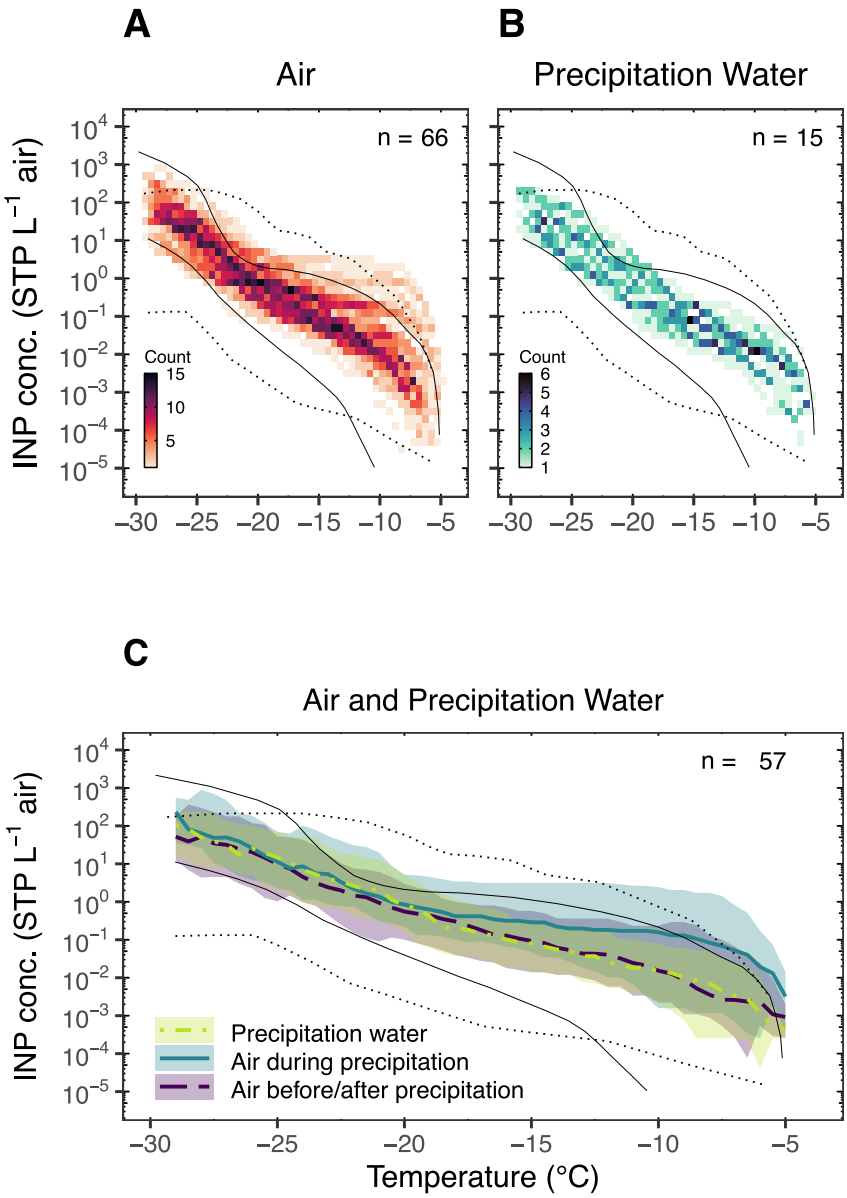

Figure 2. Cumulative ice-nucleating particle (INP) concentration as a function of freezing temperature for air and precipitation samples. Panel (a) includes all analyzed air samples collected during spring 2022 and 2023. Panel (b) is similar to panel (a) except that it includes all precipitation water samples. In panel (c), air and precipitation water samples from all 15 precipitation events are shown (see Table S1 in Supporting Information S1 summarizing all the samples). (a and b) Heat map for which the color intensity indicates the number of data points that fell within a given bin. (c) The median (thick line) and range between minimum and maximum values (light shaded area) are shown for precipitation water (dashdotted, light green), during-precipitation air (solid, blue), and pre/postprecipitation air (dashed, dark purple). In the upper right corner of each panel, the total number of samples taken into account is indicated. The dotted black lines show the envelope of observations obtained from air samples summarized by Kanji et al. (2017), while the solid thin black lines show the envelope of observations derived from precipitation samples as summarized by Petters and Wright (2015). The data from these two publications are from digitized data points extracted from the respective figures using WebPlotDigitizer (https://automeris.io/WebPlotDigitizer/, last access: 26 September 2024). Similar to Petters and Wright (2015), a cloud water content of 0.4 g m^{-3} was assumed in this study to convert INP concentrations per volume of precipitation water to STP L^{-1} air.

showed elevated concentrations of INPs active at warmer temperatures (Figure S4; Table S1 in Supporting Information S1). The median and maximum INP concentrations at −10°C in during-precipitation air were at least one order of magnitude greater than those in pre- and postprecipitation air (Figure 2c). Accordingly, the air samples mainly responsible for the pronounced hump were those collected while it was precipitating, which

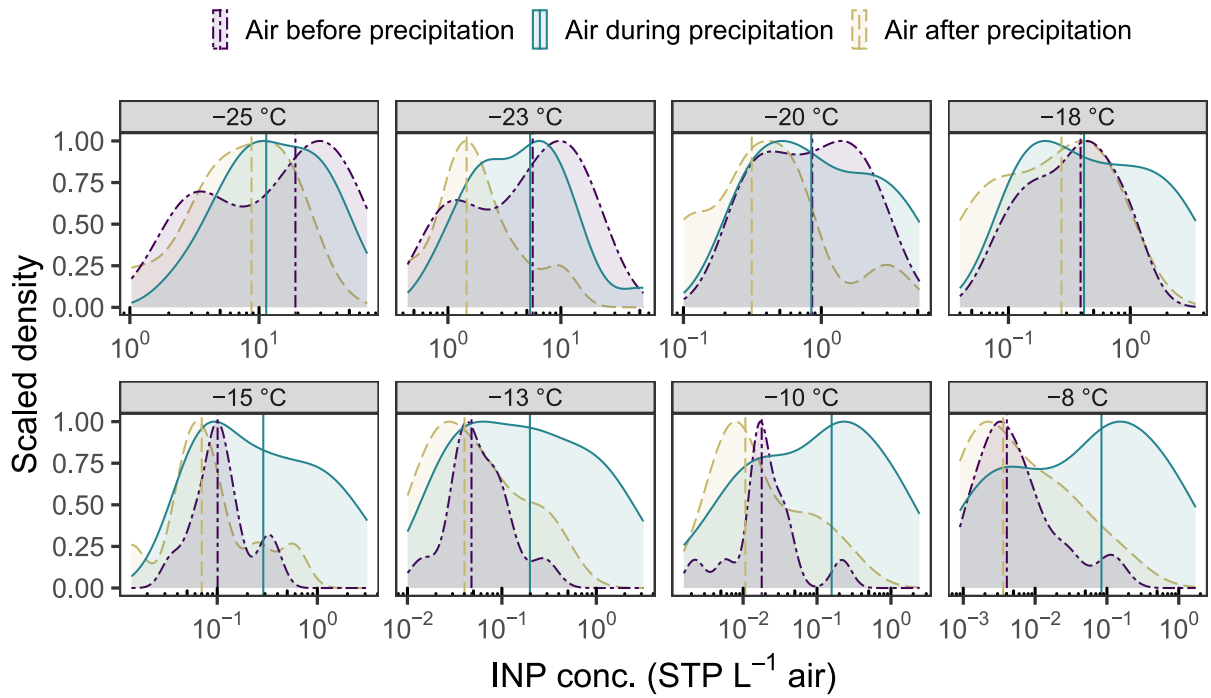

Figure 3. Scaled density functions of atmospheric ice-nucleating particle (INP) concentrations. The color and line code indicates whether the air samples were collected before ($n = 12$, dashdotted purple), during ($n = 21$, solid blue), or after ($n = 9$, dashed yellow) precipitation. The panels show data for eight INP freezing temperatures between −8°C and −25°C. Median INP concentrations are shown as vertical lines. Note that the range of the *x*-axis varies between panels.

means that atmospheric warm-temperature INPs were enhanced during precipitation. This enhancement during precipitation was especially pronounced in 2023 (Figure S5 in Supporting Information S1). Also, we found highest warm-temperature INP concentrations in 2023 for pre- and postprecipitation air samples (Figure S5 in Supporting Information S1). We note that the sample size for the comparison of INP concentrations from both years is smaller, which limits the robustness of this comparison.

The INP distribution of the precipitation water samples (Figure 2b) followed a fairly log-linear distribution over the entire temperature range. A pronounced hump was never observed. The shape of the INP distribution from precipitation water, which is independent of the scaling factor used to normalize the INP concentrations per precipitation water volume to STP L^{-1} of air, resembled that of the pre-/postprecipitation air samples (i.e., those without the pronounced hump). Assuming a content of 0.4 g cloud water per 1,000 L air to normalize the INP concentration of precipitation water (Petters & Wright, 2015), the median INP concentration of precipitation water was very similar to that of pre-/postprecipitation air along the entire temperature spectrum (Figure 2c). The similarity of the shape and median concentration of the INP distribution of precipitation water and pre-/post-precipitation air, which contrast with those of air during precipitation, suggest precipitation water, and thus, particles scavenged in and below clouds were probably a minor source of the enhanced warm-temperature INPs in air during precipitation.

The frequency distributions and medians of log-scaled INP concentrations for air before, during, and after precipitation, at eight temperatures, is shown in Figure 3. For temperatures from −8°C to −15°C, the air before precipitation had a slightly left-skewed, narrow distribution around the median with a right tail. Like the air before precipitation, the air after it typically had a left-skewed peak although with a more pronounced right tail at the warmest temperatures (>−13°C). Unlike pre-/postprecipitation air, the during-precipitation air had a broad, bimodal distribution with the right peak higher than the left one at −8°C and −10°C. For −18°C, the distributions of the three air classes were quite similar to each other. For temperatures from −20°C to −25°C, the air before precipitation had more of a right-skewed peak than air during and after precipitation. These results suggest that rain release processes (Fröhlich-Nowoisky et al., 2016) generally dominated in-cloud and below-cloud wet deposition processes (Ohata et al., 2016; Pruppacher & Klett, 2010) for warm-temperature INPs and vice versa for INPs active at colder temperatures. This is in line with findings from an agricultural site in Argentina, where the

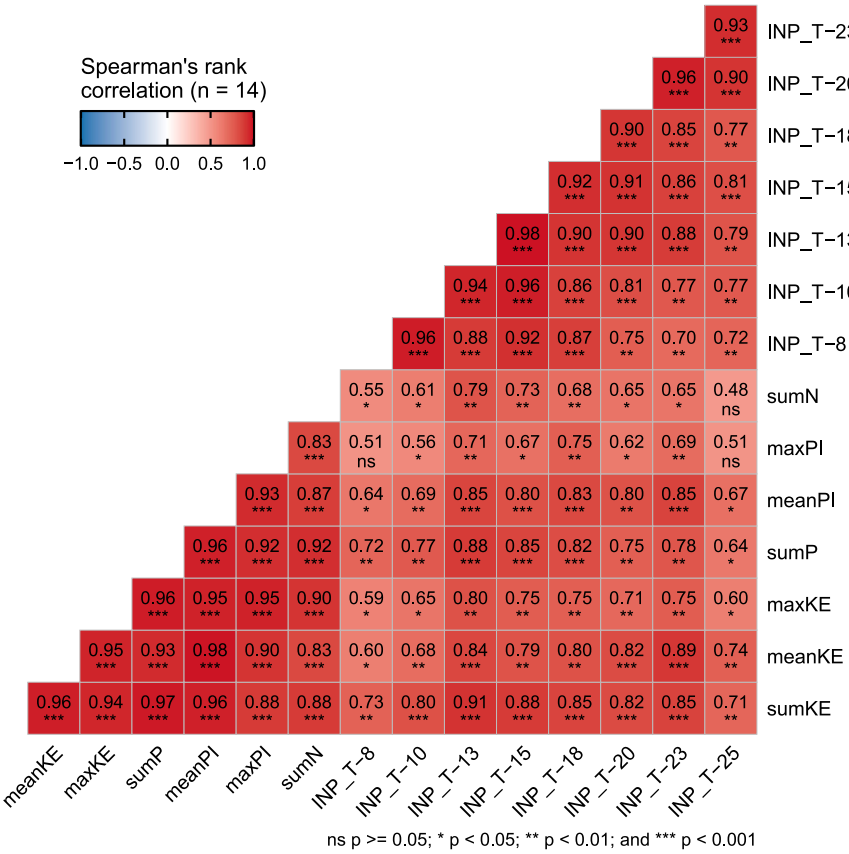

Figure 4. Spearman's rank correlation matrix of ice-nucleating particle (INP) concentrations and rainfall parameters. The matrix includes atmospheric INP concentrations at −8°C, −10°C, −13°C, −15°C, −18°C, −20°C, −23°C, and −25°C, as well as variables obtained with the disdrometer (n = 14). The number of hydrometeors (N, #), precipitation intensity (PI, mm h^{-1}), precipitation amount (P, mm), and kinetic energy (KE, J m^{-2} h^{-1}) were determined in terms of cumulative (sum), mean (mean), or maximum (max) values. The coefficients are indicated by colors and values. Different levels of correlation significance are shown by stars; nonsignificant correlations (p-value ≥ 0.05) are marked by "ns." All samples were collected during precipitation periods of the 2023 campaign.

ratio of concentrations of INPs at −12°C versus INPs at −25°C was greater for wet than dry days (Testa et al., 2021). On one hand, the rain source effect may release certain biological aerosol particles efficiently (Constantinidou et al., 1990; Kita et al., 2020) some of which may serve as warm-temperature INPs (Huffman et al., 2013). On the other hand, the wet deposition processes (i.e., sink) may affect the aerosol particle population, which reduces the INP concentrations active at warm and colder temperatures, making the overall effect of precipitation on aerosol particle populations complex and requiring further investigation (Khadir et al., 2023). We note that the warmer the nucleation temperature, the more the rain source effect was dominating the rain sink, as shown in Figure 3. Moreover, the frequency distribution of during-precipitation warm-temperature INPs was wider than preprecipitation air, which indicates that the net rain source strength varied significantly between precipitation events. Furthermore, compared to preprecipitation air, postprecipitation air was enhanced with warm-temperature INPs in a few cases. This likely depends on the trajectory of precipitating air masses, because INP concentrations can stay elevated for a couple of hours in air masses that were precipitating (Mignani et al., 2021).

3.2. Correlations Among INP Concentrations and Precipitation Parameters

Spearman correlations were calculated to determine the relationships between INP concentrations and aggregated precipitation parameters for all during-precipitation air samples and precipitation water samples for which coincident disdrometer data were available (Figure 4, Figure S8 in Supporting Information S1). These data were collected only during the 2023 campaign. We considered INP concentrations for eight different temperatures

between −8°C and −25°C, and selected precipitation-related variables, which were determined by their sum, mean, and/or maximum value for each sampling period. The variables included number of hydrometeors (N), precipitation intensity (PI, mm h^{-1}), precipitation amount (P, mm), and kinetic energy (KE, J m^{-2} h^{-1}), the latter being the KE of all the hydrometeors per measuring area and per time interval. Figure 4 reveals moderate to very strong positive (and no negative) correlations between atmospheric INP concentrations and precipitation parameters (rs = 0.48–0.91 and 61/64 correlations significant (i.e., with p-value < 0.05)). Specifically, across all temperatures analyzed, we observed the strongest correlations with cumulative KE (sum of KE for the air sampling period, sumKE) (rs = 0.71–0.91 and p-values < 0.006). Furthermore, correlations were strong with cumulative P (sumP), mean KE, maximum KE, and mean PI, and moderate with cumulative N, as well as maximum PI. In contrast, correlations between INP concentrations of the precipitation water and the precipitation parameters were neither clear nor significant (rs = −0.64–0.65 and 1/64 correlation significant, Figure S8 in Supporting Information S1). Together with the findings presented above, these results show that INPs are efficiently released into the lower atmosphere during precipitation, and that increasing values of the precipitation parameter correspond to greater atmospheric INP concentrations. The highest and lowest correlations with sumKE were found for atmospheric INPs at −13°C and −25°C, respectively. Because KE characterizes the impact force of hydrometeors on land surfaces, our results strongly suggest that the impact of raindrops and hailstones aerosolizes warm-temperature INPs from the local grassland surface. Prior studies have observed aerosolization of particles due to raindrops impacting both plant surfaces (Gilet & Bourouiba, 2014; Kim et al., 2019; Nath et al., 2019) and soils (Joung et al., 2017; Wang et al., 2016), processes sometimes referred to as "plant sneezing" and "rain splash." The latter, a well-known phenomenon in soil science research, describes how soil particles become disaggregated and detached due to raindrop impact, an initial stage of rain-induced soil erosion (Morgan, 2005).

Because sumKE exhibits the strongest correlation with INP concentration, we examined this relationship in greater detail. We also included sumP into our further analysis, as it demonstrated a significant correlation with INP concentration, and unlike other precipitation parameters, it was determined for all precipitation events (n = 15) studied here, including those in 2022.

3.3. Correlating INP Concentrations With Precipitation Amount and Rainfall Kinetic Energy

The relationships between atmospheric INP concentrations during precipitation and the two precipitation parameters sumKE and sumP are effectively captured using simple linear regression models in log-log space (Figure 5). Overall, empirical relationships between INP concentrations and sumKE and sumP were consistent and clear. The mean R-squared values across the analyzed freezing temperatures were 0.62 for sumKE and 0.44 for sumP. A rough approximation of the relationships is that a two-order-of-magnitude increase in sumKE and sumP correspond to INP concentration increases of roughly three, two, and one orders of magnitude for freezing temperatures of −8°C, −13°C, and −20°C, respectively (Figure 5).

The data points collected in 2022 (n = 4) matched well with the broader data set from both years (n = 21). However, the relationship between INP concentrations and sumP would not have been observed if only the data from 2022 had been analyzed.

Notably, two data points with the highest and second-highest sumKE (Figure 5) were associated with precipitation events involving hail, occurring on 27 May and 21 June, 2023. During these and several other events, we observed the formation of surface ponding and runoff. While we lack specific data on surface ponding, there is no indication here that partial coverage of the soil surface by water impeded a major aerosolization process. This is an indication that bare soil is a minor source of rain-induced warm-temperature INPs, particularly at the warm end, considering an entire precipitation event.

Furthermore, we identified two data points in our data set as outliers based on the visual inspection of the Cook's distance, Q–Q, and residual plots. These points had Cook's distance values close to 0.5, which were larger than those of the other data points. One outlier had the greatest INP concentrations at temperatures of −23°C and −25°C (>5 × 10^1 STP L^{-1} air), but only moderate sumKE and sumP (Figure 5). The data point was recorded during precipitation that coincided with very high wind speeds (up to a 5-min average of 13.4 m s^{-1}) at the nearby USCRN station (Diamond et al., 2013) and blowing dust/sand in the air during the passage of a front on 31 May 2023. The steep increase in INP concentration with decreasing freezing temperatures might be attributed to a substantial contribution of INPs from dust/sand particles, which were mostly active at colder temperatures, thus

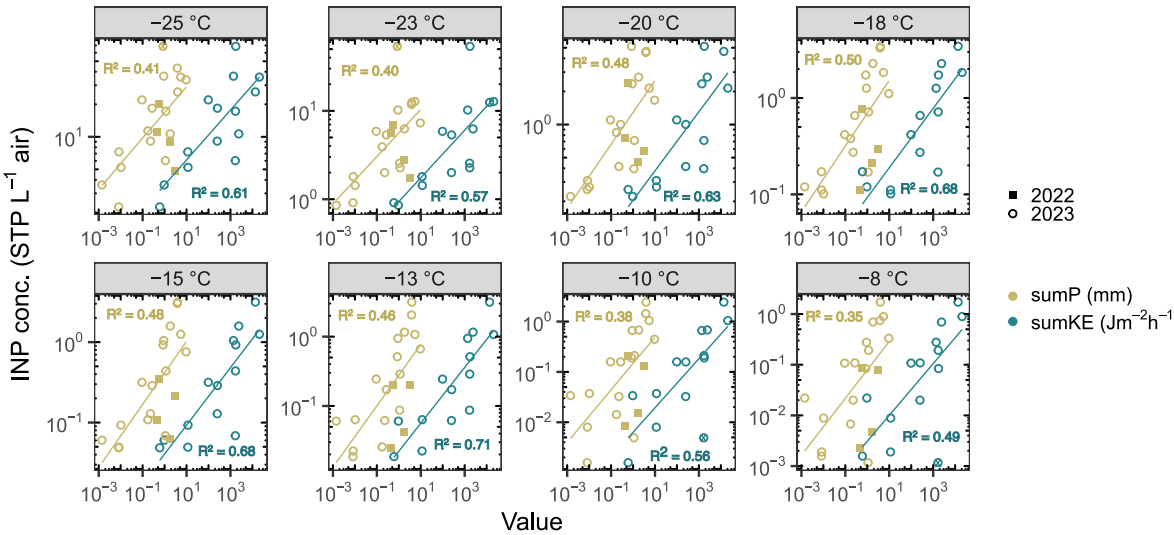

Figure 5. Ice-nucleating particle (INP) concentrations versus precipitation amount and kinetic energy (KE). Scatterplot in log-log space showing the relationship between INP concentrations (STP L^{-1} air) for during-precipitation air and cumulative precipitation amount (sumP, mm, yellow) as well as cumulative KE (sumKE, J m^{-2} h^{-1}, blue). Each panel represents INP concentrations at a different freezing temperature (from −8°C to −25°C). Symbols indicate the year of sampling (2022: filled squares and 2023: open circles). Precipitation was determined using disdrometer data ($n = 14$) or the bag method ($n = 7$), with 2022 data exclusively from the bag method. Solid lines represent linear regression models in log-log space for INP concentration versus sumP and sumKE. R-squared values of the power functions predicting during-precipitation INP concentrations based on sumP ($n = 21$) and sumKE ($n = 14$) are indicated in the upper left and the lower right corners of each panel, respectively. The identified outliers are indicated by a cross inside the circle. Note that the range of the *y*-axis varies between panels.

explaining the deviation from the regression. This aligns with the findings from Tang et al. (2022), who noted that INP populations were affected by rainfall and dust at a site in central Cyprus. Note that we found low to moderate positive Spearman correlation coefficients between during-precipitation INP concentrations and wind gusts (maximal hourly value measured during the filter collection period at the USCRN station). Highest coefficients and significant correlations ($p < 0.05$) were found for INPs active at −20°C and colder (Figure S6 in Supporting Information S1). This suggests that wind gusts do not significantly aid the enhancement of warm-temperature INPs during rainfall although they may aid the aerosolization process of cold-temperature INPs. The other outlier corresponds to a data point with higher sumKE and sumP values but lower INP concentrations at temperatures of −8°C and −10°C (<6×10^{-3} STP L^{-1} air). This anomaly occurred in the afternoon on 4 June 2023 following atypical prolonged stratiform rainfall on the day before. One speculation is that the sources of INPs available for aerosolization after prior persistent rain were already exhausted, resulting in a lack of rain-induced atmospheric INPs and suggesting a time-dependent regeneration of the INP source. Excluding this outlier resulted in higher correlation coefficients and lower p-values for the relationships between INP concentrations and all precipitation parameters (Figure S7 in Supporting Information S1).

3.4. Potential Local Terrestrial Sources of Rain-Induced INPs

One during-precipitation air sample from 27 May 2023 was selected for INP treatments (Hill et al., 2016; Suski et al., 2018) and compared to INP temperature spectra of terrestrial source samples collected at the site to infer potential sources of rain-induced INPs (Figure 6). This air sample was specifically chosen for its pronounced hump-shaped INP spectrum to obtain the best resolution of INP characteristics. The treatments revealed that the precipitation-driven hump was primarily attributable to INPs of biological origin with no significant contribution from inorganic INPs, because most INPs were labile to both, 95°C-heat and H_2O_2 digestion (Figure 6a). Several studies consistently associate the hump in INP spectra with biological particles (e.g., Barry, Hill, Levin, et al., 2021; Garcia et al., 2012; Hill et al., 2016; Knopf et al., 2021; Suski et al., 2018; Testa et al., 2021; Tobo et al., 2014). Applying the heat treatment of 50°C to the during-precipitation air sample showed that a large fraction of the detectable biological INPs were sensitive to this temperature. Several known ice-nucleating bacterial and fungal species exhibit characteristics consistent with these precipitation-induced INPs, that is, high apparent freezing onset temperature and degradation under moderate heating (temperature range here is 30–60°C): the bacteria *Pantoea agglomerans* (*Erwinia herbicola*) (Phelps et al., 1986) and *Pseudomonas sp.* (Pouleur et al., 1992), as well

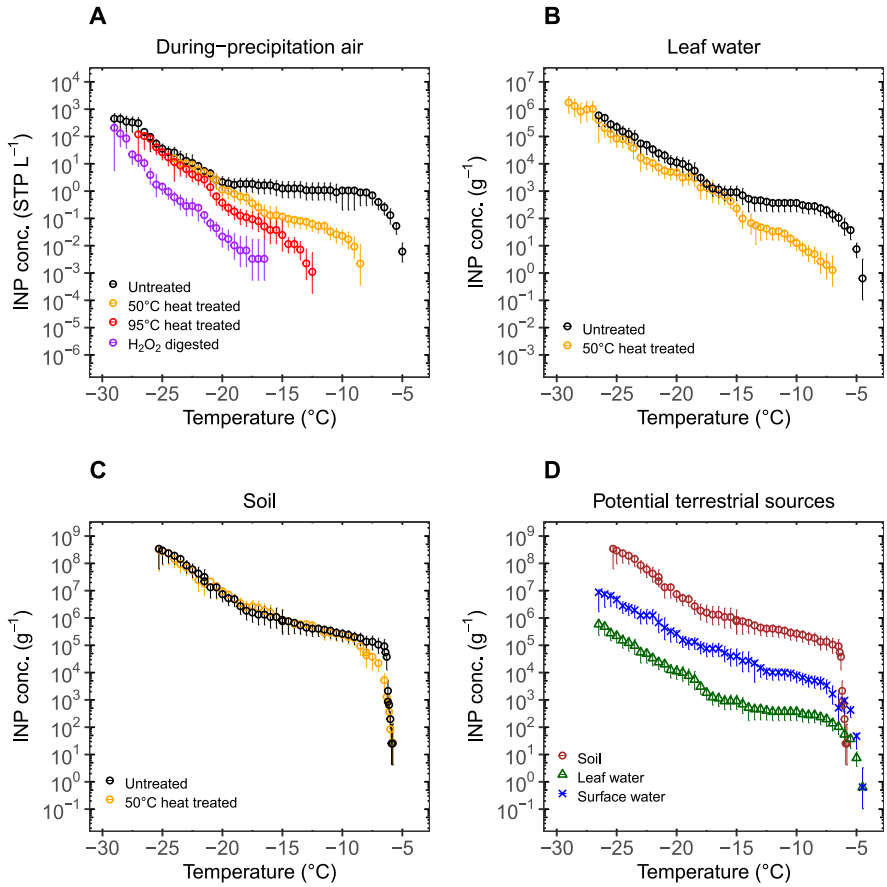

Figure 6. Cumulative ice-nucleating particle (INP) concentrations as a function of freezing temperature of selected air and terrestrial source material samples and their treatments. The effect of treatments on during-precipitation air (a), leaf water (b), and soil (c) samples are illustrated by color in panels (a–c) (untreated: black; 50°C heat treatment: orange; 95°C heat treatment: red; and H_2O_2: purple). Untreated terrestrial samples are displayed in panel (d) and differentiated by color and shape (soil: brown circles; leaf water: green triangles; surface water: blue crosses). Error bars show the 95% binomial sampling confidence intervals. INP concentrations are given in STP L^{-1} air in panel (a) and in g^{-1} of sampling material (i.e., soil, leaf water, and surface water) in panels (b–d), assuming 1 mL of surface/leaf water corresponds to 1 g thereof.

as certain *Fusarium* strains and the fungi *Acremonium implicatum* and *Isaria farinose* (Kunert et al., 2019; Pummer et al., 2015). In contrast, other species can be ruled out as potential sources of INPs active above −15°C because they retain their ice-nucleating ability after exposure to 50°C-heat (e.g., *Mortierella alpina* or *Fusarium avenaceum*) (Fröhlich-Nowoisky et al., 2015; Pummer et al., 2015). Overall, microbial INPs originating from plants tend to be heat-labile at 50–60°C, in contrast to those from soils (Conen et al., 2022). Therefore, the most likely sources of the rain-induced INPs of the air sample from 27 May 2023 are local plants. Note that below −20°C, the fraction of 95°C heat-stable INPs increased with decreasing freezing temperatures, which may indicate a shift in types and sources of INPs (i.e., toward soil organic matter) with decreasing temperature.

The shapes of INP spectra of the untreated and 50°C-heat-treated leaf water sample were similar to those of the during-precipitation air sample (Figures 6a and 6b). Both the air and leaf water samples had an apparent freezing onset temperature of about −5°C, followed by a moderate increase in concentrations over a few degrees, a shallow rate of increase between −10°C and −20°C, and an inflection point roughly around −20°C. After exposure to 50°C, a large fraction of leaf water INPs active above −17°C lost their activity, similar to what was observed for the air sample. The response to heat of the INPs in the soil sample was different from that of the air and leaf water samples. It showed a lower apparent freezing onset temperature around −6°C, followed by a steep increase within a narrow temperature range (Figure 6c). Additionally, the soil's ice-nucleating properties were largely unaffected by the 50°C heat exposure. Interestingly, the surface water sample had an INP spectrum with a shape similar to the leaf water sample, although it had more INPs per gram of material (Figure 6d). It could be that surface water

represents a mixture of INPs from leaves and soils, because INPs from leaves are washed off from plants by rain (Conen & Einbock, 2025) and soil particles are mixed into the surface water by raindrop impact (Kinnell, 1990).

All terrestrial materials analyzed here contained large amounts of warm-temperature INPs, which could have contributed as sources of INPs to the atmosphere. More specifically, the results of a few samples suggest that the source of the majority of airborne, rain-induced INPs observed during one precipitation event, especially those active above −15°C, was likely dominated by plant leaves rather than by soil sources. Such dominance was noted in wildfire emissions (Barry, Hill, Levin, et al., 2021) and at a high-altitude site (Einbock & Conen, 2024); evidence is accumulating of a common source of warm-temperature INPs being from plant sources. It is plausible that INPs from leaves could have been released into the atmosphere when raindrops and hailstones impacted the leaves or the surface water.

4. Conclusions

In 2022 and 2023, we performed high-time-resolution near-surface INP measurements at a semiarid site, with targeted sampling before, during, and after 15 rainfall events, including three hail storms. Air, precipitation water, and terrestrial samples were collected for INP analysis in parallel with coinciding ground-based wind and rainfall observations. Consistent with previous findings, we observed generally more INPs active above −20°C (i.e., warm-temperature INPs) in the air during precipitation than both pre- and postprecipitation conditions (Bigg, 1958; Conen et al., 2017; Gong et al., 2022; Hara et al., 2016; Huffman et al., 2013; Isono & Tanaka, 1966; Mignani et al., 2021; Prenni et al., 2013; Ryan & Scott, 1969; Testa et al., 2021; Tobo et al., 2013). Moreover, we found that during-precipitation atmospheric INP concentrations positively correlated with the assessed weather and rainfall parameters. Among these, cumulative rainfall KE (sumKE)—derived from disdrometer measurements (Löffler-Mang & Joss, 2000)—showed the strongest correlations with INP concentrations for each of the analyzed activation temperatures, with the highest correlation coefficient observed for INPs at −13°C (Spearman's $r = 0.91$, $p < 0.001$, and $n = 14$). To our knowledge, this is the first study to compare ambient INP concentrations with detailed rainfall microphysics.

Comparing INP spectra from air samples with samples of precipitation water (converted to per L air (Petters & Wright, 2015)) revealed a close resemblance between the median spectra of precipitation water and the air from pre- or postprecipitation. This suggests the precipitation water, and thus, particles scavenged from the air within and below precipitating clouds were relatively minor sources of the elevated warm-temperature INPs in the lower atmosphere during precipitation. Additionally, INP treatments (Hill et al., 2016; Suski et al., 2018) of four selected samples (air, soil, surface water, and leaf water) showed that during-precipitation warm-temperature atmospheric INPs lost their ice-nucleating activity after 50°C heat treatment, resembling the behavior of INPs derived from plant leaf water in this study and the general expectations of certain bacterial and fungal INPs (Conen et al., 2022). This contrasted with the 50°C resilience of soil INPs from the site and with general expectations for INPs emanating from pollen or their fragments, and some fungal INPs (Conen et al., 2022). Taken together, our results provide compelling evidence for a pathway in which biological INPs are detached from local terrestrial surfaces by the impact of raindrops and hailstones, considerably enhancing warm-temperature INPs in the local air during the immediate period of rain and shortly thereafter. These findings significantly improve our understanding of the emission pathway of INPs during rainfall.

Pre- and postprecipitation INP concentrations are likely a result of dilution and the attenuation or absence of the rain-driven source in the air masses arriving at the measurement site. Nevertheless, rain-induced particles emitted from the surface can be expected to be transported vertically and potentially reach cloud level, particularly given that surface aerosol properties are well correlated with those in the boundary layer (Delle Monache et al., 2004). This condition is particularly plausible during rainy conditions, which are often accompanied by strong winds, as frequently observed in the High Plains during late spring (Smith et al., 2013). However, vertical transport studies are needed to assess the flux of rain-induced particles to cloud-relevant heights. To address this, we recommend combining large air volume sampling with short, targeted observation windows to capture emission events, and vertical profiling using towers, balloons, or drone systems.

In this study, samples were taken in two spring seasons. The current data set remains too small to draw conclusions regarding interannual differences. Nonetheless, the contrasting precipitation frequency and amount, and thus the vegetation cover in both springs at the measurement site (see Figure 1) could have influenced local biological aerosol particle and INP emissions. While we chose a native grassland site in Colorado and primarily

targeted short-lived convective storms, a broader assessment of precipitation-related INP emissions across different land covers, seasons, years, and storm types is needed. In addition, a larger number of terrestrial samples, including especially samples of different plant species, would be useful in future studies to better determine and understand the source of rain-induced INPs.

Our results document a link between the concentrations of atmospheric INPs during rain and their emission pathway. They also suggest that rainfall parameters are reasonable for predicting atmospheric INP concentrations during rainfall, assuming that possible other parameters possibly influencing the relationship between rainfall and INPs (e.g., land cover and storm type) are known. Because aerosolization of INPs may require some level of KE, sumKE may represent a potential robust predictor of rainfall-induced INP emissions. For convective storms, for which sumKE and cumulative precipitation amount (sumP) strongly correlate, sumP might be a reliable predictor as well. Given that the latter is a routinely recorded meteorological parameter and does not require advanced precipitation measurement techniques, it maybe a more practical predictor. Ultimately, this study supports considering including rainfall as a driver for INPs in relevant parameterizations and numerical cloud models. Such implementations, together with vertical profiling observation, will be useful to quantify precipitation-induced INPs within clouds and further improve our understanding of aerosol-cloud-precipitation interactions.

Data Availability Statement

The INP data of this study are archived on the NCAR Earth Observing Laboratory Data Archive pages at https://data.eol.ucar.edu/dataset/648.003 (Mignani et al., 2025). The INP data from Petters and Wright (2015) and Kanji et al. (2017) were extracted from the respective figures using WebPlotDigitizer. Meteorological data from the USCRN station near Nunn, CO, were provided by the National Centers for Environmental Information (NCEI) (Diamond et al., 2013). Monthly precipitation data and 5-min average wind speed data were obtained from the following website: https://www.ncei.noaa.gov/pub/data/uscrn/products/. The respective data sets were selected based on the time resolution, year, and the station near Nunn (i.e., https://www.ncei.noaa.gov/pub/data/uscrn/products/monthly01/CRNM0102-CO_Nunn_7_NNE.txt and https://www.ncei.noaa.gov/pub/data/uscrn/products/subhourly01/2023/CRNS0101-05-2023-CO_Nunn_7_NNE.txt). Wind gust data were obtained from https://mesowest.utah.edu. Historical precipitation data were downloaded from the WorldClim data website (Fick & Hijmans, 2017).

Acknowledgments

We would like to acknowledge the support from the U.S. Department of Agriculture agency of Agricultural Research Service for providing access to the CPER. We thank Amy Bibbey and Troy Bauder and other staff at the Colorado Agricultural Experiment Station for their help in supporting and scheduling facilities at the SGRC. Our sincere thanks go to all members of BACS and BROADN for the various assistance during the measurement campaigns and fruitful discussions along the study. Special thanks to Alexandra C. Mazurek, Jacob A. Escobedo, Nicholas M. Falk, Christine A. Neumaier, and Ben D. Ascher for their excellent daily weather forecasts during the campaigns. We are grateful for OTTHydroMet's technical service and their support with the disdrometer. Claudia Mignani would like to express her profound gratitude to Pedro Batista for his tireless support during the fieldwork and valuable insights into soil erosion. Furthermore, she is grateful for the exchange with colleagues at the Pacific Northwest National Laboratory and at the Karlsruhe Institute of Technology. Finally, we acknowledge support from the National Science Foundation through funding BACS (AGS-2105938 and AGS-2106370), BROADN (DBI-2120117), and the NEON Program. Note that the NEON Program is operated under cooperative agreement by Battelle. Also, the BACS and BROADN campaigns were supported by the NEON Assignable Assets program. In addition, we thank the Swiss National Science Foundation for support through the Postdoc.Mobility grant (P500PN_206661) as well as the One Health Institute at Colorado State University.

References

Barry, K. R., Hill, T. C., Jentzsch, C., Moffett, B. F., Stratmann, F., & DeMott, P. J. (2021). Pragmatic protocols for working cleanly when measuring ice nucleating particles. *Atmospheric Research*, *250*, 105419. https://doi.org/10.1016/j.atmosres.2020.105419

Barry, K. R., Hill, T. C. J., Levin, E. J. T., Twohy, C. H., Moore, K. A., Weller, Z. D., et al. (2021). Observations of ice nucleating particles in the free troposphere from Western US wildfires. *Journal of Geophysical Research: Atmospheres*, *126*(3), e2020JD033752. https://doi.org/10.1029/2020JD033752

Beall, C. M., Michaud, J. M., Fish, M. A., Dinasquet, J., Cornwell, G. C., Stokes, M. D., et al. (2021). Cultivable halotolerant ice-nucleating bacteria and fungi in coastal precipitation. *Atmospheric Chemistry and Physics*, *21*(11), 9031–9045. https://doi.org/10.5194/acp-21-9031-2021

Bigg, E. K. (1958). A long period fluctuation in freezing nucleus concentrations. *Journal of the Atmospheric Sciences*, *15*(6), 561–562. https://doi.org/10.1175/1520-0469(1958)015<0561:ALPFIF>2.0.CO;2

Bigg, E. K., Soubeyrand, S., & Morris, C. E. (2015). Persistent after-effects of heavy rain on concentrations of ice nuclei and rainfall suggest a biological cause. *Atmospheric Chemistry and Physics*, *15*(5), 2313–2326. https://doi.org/10.5194/acp-15-2313-2015

Burrows, S. M., McCluskey, C. S., Cornwell, G., Steinke, I., Zhang, K., Zhao, B., et al. (2022). Ice-nucleating particles that impact clouds and climate: Observational and modeling research needs. *Reviews of Geophysics*, *60*(2). https://doi.org/10.1029/2021RG000745

Conen, F., Eckhardt, S., Gundersen, H., Stohl, A., & Yttri, K. E. (2017). Rainfall drives atmospheric ice-nucleating particles in the coastal climate of southern Norway. *Atmospheric Chemistry and Physics*, *17*(18), 11065–11073. https://doi.org/10.5194/acp-17-11065-2017

Conen, F., & Einbock, A. (2025). Release of ice-nucleating particles from leaves during rainfall. *Science and Nature*, *112*(2), 29. https://doi.org/10.1007/s00114-025-01980-6

Conen, F., Einbock, A., Mignani, C., & Hüglin, C. (2022). Measurement report: Ice-nucleating particles active ≥ −15 °C in free tropospheric air over western Europe. *Atmospheric Chemistry and Physics*, *22*(5), 3433–3444. https://doi.org/10.5194/acp-22-3433-2022

Constantinidou, H. A., Hirano, S. S., Baker, L. S., & Upper, C. D. (1990). Atmospheric dispersal of ice nucleation-active bacteria: The role of rain. *Phytopathology*, *80*(10), 934–937. https://doi.org/10.1094/phyto-80-934

Cornwell, G. C., McCluskey, C. S., Hill, T. C., Levin, E. T., Rothfuss, N. E., Tai, S.-L., et al. (2023). Bioaerosols are the dominant source of warm-temperature immersion-mode INPs and drive uncertainties in INP predictability. *Science Advances*, *9*(37), eadg3715. https://doi.org/10.1126/sciadv.adg3715

Delle Monache, L., Perry, K. D., Cederwall, R. T., & Ogren, J. A. (2004). In situ aerosol profiles over the Southern Great Plains cloud and radiation test bed site: 2. Effects of mixing height on aerosol properties. *Journal of Geophysical Research*, *109*(D6), D06209. https://doi.org/10.1029/2003JD004024

DeMott, P. J., Möhler, O., Cziczo, D. J., Hiranuma, N., Petters, M. D., Petters, S. S., et al. (2018). The Fifth International Workshop on Ice Nucleation phase 2 (FIN-02): Laboratory intercomparison of ice nucleation measurements. *Atmospheric Measurement Techniques*, *11*, 6231–6257. https://doi.org/10.5194/amt-11-6231-2018

DeMott, P. J., & Prenni, A. J. (2010). New Directions: Need for defining the numbers and sources of biological aerosols acting as ice nuclei. *Atmospheric Environment*, *44*(15), 1944–1945. https://doi.org/10.1016/j.atmosenv.2010.02.032

DeMott, P. J., Prenni, A. J., Liu, X., Kreidenweis, S. M., Petters, M. D., Twohy, C. H., et al. (2010). Predicting global atmospheric ice nuclei distributions and their impacts on climate. *Proceedings of the National Academy of Sciences of the United States of America*, *107*(25), 11217–11222. https://doi.org/10.1073/pnas.0910818107

Diamond, H. J., Karl, T. R., Palecki, M. A., Baker, C. B., Bell, J. E., Leeper, R. D., et al. (2013). U.S. climate reference network after one decade of operations: Status and assessment. *Bulletin of the American Meteorological Society*, *94*(4), 485–498. https://doi.org/10.1175/BAMS-D-12-00170.1

Dolan, B., Fuchs, B., Rutledge, S. A., Barnes, E. A., & Thompson, E. J. (2018). Primary modes of global drop size distributions. *Journal of the Atmospheric Sciences*, *75*(5), 1453–1476. https://doi.org/10.1175/JAS-D-17-0242.1

Einbock, A., & Conen, F. (2024). Similar freezing spectra of particles in plant canopies and in the air at a high-altitude site. *Biogeosciences*, *21*(22), 5219–5231. https://doi.org/10.5194/bg-21-5219-2024

Fick, S. E., & Hijmans, R. J. (2017). WorldClim 2: New 1-km spatial resolution climate surfaces for global land areas. *International Journal of Climatology*, *37*(12), 4302–4315. https://doi.org/10.1002/joc.5086

Fischer, E., & Knutti, R. (2016). Observed heavy precipitation increase confirms theory and early models. *Nature Climate Change*, *6*(11), 986–991. https://doi.org/10.1038/nclimate3110

Fröhlich-Nowoisky, J., Hill, T. C. J., Pummer, B. G., Yordanova, P., Franc, G. D., & Pöschl, U. (2015). Ice nucleation activity in the widespread soil fungus Mortierella alpina. *Biogeosciences*, *12*(4), 1057–1071. https://doi.org/10.5194/bg-12-1057-2015

Fröhlich-Nowoisky, J., Kampf, C. J., Weber, B., Huffman, J. A., Pöhlker, C., Andreae, M. O., et al. (2016). Bioaerosols in the Earth system: Climate, health, and ecosystem interactions. *Atmospheric Research*, *182*, 346–376. https://doi.org/10.1016/j.atmosres.2016.07.018

Garcia, E., Hill, T. C. J., Prenni, A. J., DeMott, P. J., Franc, G. D., & Kreidenweis, S. M. (2012). Biogenic ice nuclei in boundary layer air over two U.S. High Plains agricultural regions. *Journal of Geophysical Research*, *117*(D18), D18209. https://doi.org/10.1029/2012JD018343

Gilet, T., & Bourouiba, L. (2014). Rain-induced ejection of pathogens from leaves: Revisiting the hypothesis of splash-on-film using high-speed visualization. *Integrative and Comparative Biology*, *54*(6), 974–984. https://doi.org/10.1093/icb/icu116

Gong, X., Radenz, M., Wex, H., Seifert, P., Ataei, F., Henning, S., et al. (2022). Significant continental source of ice-nucleating particles at the tip of Chile's southernmost Patagonia region. *Atmospheric Chemistry and Physics*, *22*(16), 10505–10525. https://doi.org/10.5194/acp-22-10505-2022

Hara, K., Maki, T., Kobayashi, F., Kakikawa, M., Wada, M., & Matsuki, A. (2016). Variations of ice nuclei concentration induced by rain and snowfall within a local forested site in Japan. *Atmospheric Environment*, *127*, 1–5. https://doi.org/10.1016/j.atmosenv.2015.12.009

Hill, T. C. J., DeMott, P. J., Tobo, Y., Fröhlich-Nowoisky, J., Moffett, B. F., Franc, G. D., & Kreidenweis, S. M. (2016). Sources of organic ice nucleating particles in soils. *Atmospheric Chemistry and Physics*, *16*(11), 7195–7211. https://doi.org/10.5194/acp-16-7195-2016

Hirano, S. S., Baker, L. S., & Upper, C. D. (1996). Raindrop momentum triggers growth of leaf-associated population of *Pseudomonas syringae* on field-grown snap bean plants. *Applied and Environmental Microbiology*, *62*(7), 2560–2566. https://doi.org/10.1128/aem.62.7.2560-2566

Huang, S., Hu, W., Chen, J., Wu, Z., Zhang, D., & Fu, P. (2021). Overview of biological ice nucleating particles in the atmosphere. *Environment International*, *146*, 106–197. https://doi.org/10.1016/j.envint.2020.106197

Huffman, J. A., Prenni, A. J., DeMott, P. J., Pöhlker, C., Mason, R. H., Robinson, N. H., et al. (2013). High concentrations of biological aerosol particles and ice nuclei during and after rain. *Atmospheric Chemistry and Physics*, *13*, 6151–6164. https://doi.org/10.5194/acp-13-6151-2013

Isaac, G. A., & Douglas, R. H. (1973). Ice nucleus concentrations at −20 °C during convective storms. *Journal of Applied Meteorology*, *12*(7), 1183–1190. https://doi.org/10.1175/1520-0450(1973)012<1183:incadc>2.0.co;2

Isono, K., & Tanaka, T. (1966). Sudden increase of ice nucleus concentration associated with thunderstorm. *Journal of the Meteorological Society of Japan*, *44*(5), 255–259. https://doi.org/10.2151/jmsj1965.44.5_255

Joung, Y. S., Ge, Z., & Buie, C. R. (2017). Bioaerosol generation by raindrops on soil. *Nature Communications*, *8*(1), 14668. https://doi.org/10.1038/ncomms14668

Kanji, Z. A., Ladino, L. A., Wex, H., Boose, Y., Burkert-Kohn, M., Cziczo, D. J., & Krämer, M. (2017). Overview of ice nucleating particles. *Meteorological Monographs*, *58*, 1.1–1.33. https://doi.org/10.1175/AMSMONOGRAPHS-D-16-0006.1

Khadir, T., Riipinen, I., Talvinen, S., Heslin-Rees, D., Pöhlker, C., Rizzo, L., et al. (2023). Sink, source or something in-between? Net effects of precipitation on aerosol particle populations. *Geophysical Research Letters*, *50*(19), e2023GL104325. https://doi.org/10.1029/2023GL104325

Kim, S., Park, H., Gruszewski, H. A., Schmale, D. G., & Jung, S. (2019). Vortex-induced dispersal of a plant pathogen by raindrop impact. *Proceedings of the National Academy of Sciences of the United States of America*, *116*(11), 4917–4922. https://doi.org/10.1073/pnas.1820318116

Kinnell, P. I. A. (1990). The mechanics of raindrop induced flow transport. *Australian Journal of Soil Research*, *28*(4), 497–516. https://doi.org/10.1071/SR9900497

Kita, K., Igarashi, Y., Kinase, T., Hayashi, N., Ishizuka, M., Adachi, K., et al. (2020). Rain-induced bioecological resuspension of radiocaesium in a polluted forest in Japan. *Scientific Reports*, *10*(1), 15330. https://doi.org/10.1038/s41598-020-72029-z

Knopf, D. A., Barry, K. R., Brubaker, T. A., Jahl, L. G., Jankowski, K. A., Li, J., et al. (2021). Aerosol–ice formation closure: A Southern Great Plains field campaign. *Bulletin of the American Meteorological Society*, *102*(10), E1952–E1971. https://doi.org/10.1175/BAMS-D-20-0151.1

Korolev, A., & Leisner, T. (2020). Review of experimental studies of secondary ice production. *Atmospheric Chemistry and Physics*, *20*, 11767–11797. https://doi.org/10.5194/acp-20-11767-2020

Krajewski, W. F., Ciach, G. J., & Habib, E. (2003). An analysis of small-scale rainfall variability in different climatic regimes. *Hydrological Sciences Journal*, *48*(2), 151–162. https://doi.org/10.1623/hysj.48.2.151.44694

Kunert, A. T., Pöhlker, M. L., Tang, K., Krevert, C. S., Wieder, C., Speth, K. R., et al. (2019). Macromolecular fungal ice nuclei in *Fusarium*: Effects of physical and chemical processing. *Biogeosciences*, *16*(23), 4647–4659. https://doi.org/10.5194/bg-16-4647-2019

Lindow, S. E., Lahue, E., Govindarajan, A. G., Panopoulos, N. J., & Gies, D. (1989). Localization of ice nucleation activity and the *iceC* gene product in *Pseudomonas syringae* and *Escherichia coli*. *Molecular Plant-Microbe Interactions*, *2*(5), 262–272. https://doi.org/10.1094/mpmi-2-262

Löffler-Mang, M., & Joss, J. (2000). An optical disdrometer for measuring size and velocity of hydrometeors. *Journal of Atmospheric and Oceanic Technology*, *17*(2), 130–139. https://doi.org/10.1175/1520-0426(2000)017<0130:AODFMS>2.0.CO;2

Metzger, S., Ayres, E., Durden, D., Florian, C., Lee, R., Lunch, C., et al. (2019). From NEON field sites to data portal: A community resource for surface–atmosphere research comes online. *Bulletin of the American Meteorological Society*, *100*(11), 2305–2325. https://doi.org/10.1175/BAMS-D-17-0307.1

Mignani, C., Hill, T. C. J., Nieto-Caballero, M., Barry, K. R., Bryan, N. C., Marinescu, P. J., et al. (2025). BACS: Semi-arid Grassland Research Center Ice-Nucleating Particle (SGRC-INP) All. Version 1.0. *UCAR/NCAR - Earth Observing Laboratory*. https://doi.org/10.26023/KAD2-23NZ-DN03

Mignani, C., Wieder, J., Sprenger, M. A., Kanji, Z. A., Henneberger, J., Alewell, C., & Conen, F. (2021). Towards parameterising atmospheric concentrations of ice-nucleating particles active at moderate supercooling. *Atmospheric Chemistry and Physics*, *21*(2), 657–664. https://doi.org/10.5194/acp-21-657-2021

Morgan, R. P. C. (2005). *Soil erosion and conservation* (3rd ed.). Blackwell Publishing.

Morris, C. E., Conen, F., Alex Huffman, J., Phillips, V., Pöschl, U., & Sands, D. C. (2014). Bioprecipitation: A feedback cycle linking Earth history, ecosystem dynamics and land use through biological ice nucleators in the atmosphere. *Global Change Biology*, *20*(2), 341–351. https://doi.org/10.1111/gcb.12447

Morris, C. E., Soubeyrand, S., Bigg, E. K., Creamean, J. M., & Sands, D. C. (2017). Mapping rainfall feedback to reveal the potential sensitivity of precipitation to biological aerosols. *Bulletin of the American Meteorological Society*, *98*(6), 1109–1118. https://doi.org/10.1175/BAMS-D-15-00293.1

Mülmenstädt, J., Sourdeval, O., Delanoë, J., & Quaas, J. (2015). Frequency of occurrence of rain from liquid-mixed-and ice-phase clouds derived from A-Train satellite retrievals. *Geophysical Research Letters*, *42*(15), 6502–6509. https://doi.org/10.1002/2015GL064604

Murray, B. J., O'Sullivan, D., Atkinson, J., & Webb, M. E. (2012). Ice nucleation by particles immersed in supercooled cloud droplets. *Chemical Society Reviews*, *41*(19), 6519–6554. https://doi.org/10.1039/C2CS35200A

Nath, S., Ahmadi, S. F., Gruszewski, H. A., Budhiraja, S., Bisbano, C. E., Jung, S., et al. (2019). "Sneezing" plants: Pathogen transport via jumping-droplet condensation. *Journal of The Royal Society Interface*, *16*(155), 20190243. https://doi.org/10.1098/rsif.2019.0243

Ohata, S., Moteki, N., Mori, T., Koike, M., & Kondo, Y. (2016). A key process controlling the wet removal of aerosols: New observational evidence. *Scientific Reports*, *6*(1), 34113. https://doi.org/10.1038/srep34113

OTT HydroMet. (2017). Operating instructions present weather sensor OTT Parsivel^2 (with screen heating) (p. 52). Retrieved from https://www.ott.com/resources/

Pereira Freitas, G., Adachi, K., Conen, F., Heslin-Rees, D., Krejci, R., Tobo, Y., et al. (2023). Regionally sourced bioaerosols drive high-temperature ice nucleating particles in the Arctic. *Nature Communications*, *14*(1), 5997. https://doi.org/10.1038/s41467-023-41696-7

Perkins, R. J., Gillette, S. M., Hill, T. C. J., & DeMott, P. J. (2020). The labile nature of ice nucleation by Arizona test dust. *ACS Earth and Space Chemistry*, *4*(1), 133–141. https://doi.org/10.1021/acsearthspacechem.9b00304

Petters, M. D., & Wright, T. P. (2015). Revisiting ice nucleation from precipitation samples. *Geophysical Research Letters*, *42*(20), 8758–8766. https://doi.org/10.1002/2015GL065733

Phelps, P., Giddings, T. H., Prochoda, M., & Fall, R. (1986). Release of cell-free ice nuclei by *Erwinia herbicola*. *Journal of Bacteriology*, *167*(2), 492–502. https://doi.org/10.1128/jb.167.2.496-502.1986

Pouleur, S., Richard, C., Martin, J. G., & Antoun, H. (1992). Ice nucleation activity in *Fusarium acuminatum* and *Fusarium avenaceum*. *Applied and Environmental Microbiology*, *59*(9), 2960–2964. https://doi.org/10.1128/aem.58.9.2960-2964.1992

Prenni, A. J., Tobo, Y., Garcia, E., DeMott, P. J., Huffman, J. A., McCluskey, C. S., et al. (2013). The impact of rain on ice nuclei populations at a forested site in Colorado. *Geophysical Research Letters*, *40*(1), 227–231. https://doi.org/10.1029/2012GL053953

Pruppacher, H. R., & Klett, J. D. (2010). Microphysics of clouds and precipitation. In *Second revised and expanded edition with an introduction to cloud chemistry and cloud electricity*. Springer. https://doi.org/10.1007/978-0-306-48100-0

Pummer, B. G., Budke, C., Augustin-Bauditz, S., Niedermeier, D., Felgitsch, L., Kampf, C. J., et al. (2015). Ice nucleation by water-soluble macromolecules. *Atmospheric Chemistry and Physics*, *15*(8), 4077–4091. https://doi.org/10.5194/acp-15-4077-2015

Ryan, B. F., & Scott, W. D. (1969). Ice nuclei and the onset of rainfall. *Journal of the Atmospheric Sciences*, *26*(3), 611–612. https://doi.org/10.1175/1520-0469(1969)026<0611:INATOO>2.0.CO;2

Sands, D. C., Langhans, V. E., Scharen, A. L., & de Smet, G. (1982). The association between bacteria and rain and possible resultant meteorological implications. *Idojaras*, *86*, 148–152.

Schneider, J., Höhler, K., Heikkilä, P., Keskinen, J., Bertozzi, B., Bogert, P., et al. (2021). The seasonal cycle of ice-nucleating particles linked to the abundance of biogenic aerosol in boreal forests. *Atmospheric Chemistry and Physics*, *21*(5), 3899–3918. https://doi.org/10.5194/acp-21-3899-2021

Smith, B. T., Castellanos, T. E., Winters, A. C., Mead, C. M., Dean, A. R., & Thompson, R. L. (2013). Measured severe convective wind climatology and associated convective modes of thunderstorms in the contiguous United States, 2003–09. *Weather and Forecasting*, *28*(1), 229–236. https://doi.org/10.1175/WAF-D-12-00096.1

Soubeyrand, S., Morris, C. E., & Bigg, E. K. (2014). Analysis of fragmented time directionality in time series to elucidate feedbacks in climate data. *Environmental Modelling & Software*, *61*, 78–86. https://doi.org/10.1016/j.envsoft.2014.07.003

Soulage, G. (1957). Les noyaux de congélation de l'atmosphère. *Annals of Geophysics*, *13*, 103–143.

Spurny, K. R., & Lodge, J. P., Jr. (1972). Collection efficiency tables for membrane filters used in the sampling and analysis of aerosols and hydrosols. *NCAR Technical Note*. https://doi.org/10.5065/D6F769JJ

Suski, K. J., Hill, T. C. J., Levin, E. J. T., Miller, A., DeMott, P. J., & Kreidenweis, S. M. (2018). Agricultural harvesting emissions of ice-nucleating particles. *Atmospheric Chemistry and Physics*, *18*, 13755–13771. https://doi.org/10.5194/acp-18-13755-2018

Tang, K., Sánchez-Parra, B., Yordanova, P., Wehking, J., Backes, A. T., Pickersgill, D. A., et al. (2022). Bioaerosols and atmospheric ice nuclei in a mediterranean dryland: Community changes related to rainfall. *Biogeosciences*, *19*(1), 71–91. https://doi.org/10.5194/bg-19-71-2022

Testa, B., Hill, T. C. J., Marsden, N. A., Barry, K. R., Hume, C. C., Bian, Q., et al. (2021). Ice nucleating particle connections to regional Argentinian land surface emissions and weather during the Cloud, Aerosol, and Complex Terrain Interactions Experiment. *Journal of Geophysical Research: Atmospheres*, *126*(23), e2021JD035186. https://doi.org/10.1029/2021JD035186

Tobo, Y., DeMott, P. J., Hill, T. C. J., Prenni, A. J., Swoboda-Colberg, N. G., Franc, G. D., & Kreidenweis, S. M. (2014). Organic matter matters for ice nuclei of agricultural soil origin. *Atmospheric Chemistry and Physics*, *14*(16), 8521–8531. https://doi.org/10.5194/acp-14-8521-2014

Tobo, Y., Prenni, A. J., DeMott, P. J., Huffman, J. A., McCluskey, C. S., Tian, G., et al. (2013). Biological aerosol particles as a key determinant of ice nuclei populations in a forest ecosystem. *Journal of Geophysical Research: Atmospheres*, *118*(17), 10100–10110. https://doi.org/10.1002/jgrd.50801

Tokay, A., Wolff, D. B., & Petersen, W. A. (2014). Evaluation of the new version of the laser-optical disdrometer, OTT Parsivel^2. *Journal of Atmospheric and Oceanic Technology*, *31*(6), 1276–1288. https://doi.org/10.1175/JTECH-D-13-00174.1

Vali, G. (1971). Supercooling of water and nucleation of ice (drop freezer). *American Journal of Physics*, *39*(10), 1125–1128. https://doi.org/10.1119/1.1976585

Wang, B., Harder, T. H., Kelly, S. T., Piens, D. S., China, S., Kovarik, L., et al. (2016). Airborne soil organic particles generated by precipitation. *Nature Geoscience*, *9*(6), 433–437. https://doi.org/10.1038/NGEO2705

Wilken, F., Baur, M., Sommer, M., Deumlich, D., Bens, O., & Fiener, P. (2018). Uncertainties in rainfall kinetic energy-intensity relations for soil erosion modelling. *Catena (Cremlingen)*, *171*, 234–244. https://doi.org/10.1016/j.catena.2018.07.002

Wolber, P. K., Deininger, C. A., Southworth, M. W., Vandekerckhove, J., van Montagu, M., & Warren, G. (1986). Identification and purification of a bacterial ice-nucleation protein. *Proceedings of the National Academy of Sciences of the United States of America*, *83*(19), 7256–7260. https://doi.org/10.1073/pnas.83.19.7256